Simulation of the West African monsoon onset using the HadGEM3-RA regional climate model

Ismaïla Diallo · Caroline L. Bain · Amadou T. Gaye ·
Wilfran Moufouma-Okia · Coumba Niang ·
Mame D. B. Dieng · Richard Graham

Abstract The performance of the Hadley Centre Global Environmental Model version 3 regional climate model (HadGEM3-RA) in simulating the West African monsoon (WAM) is investigated. We focus on performance for monsoon onset timing and for rainfall totals over the June–July–August (JJA) season and on the model's representation of the underlying dynamical processes. Experiments are driven by the ERA-Interim reanalysis and follow the CORDEX experimental protocol. Simulations with the HadGEM3 global model, which shares a common physical formulation with HadGEM3-RA, are used to gain insight into the causes of HadGEM3-RA simulation errors. It is found that HadGEM3-RA simulations of monsoon onset timing are realistic, with an error in mean onset date of two pentads. However, the model has a dry bias over the Sahel during JJA of 15–20 %. Analysis suggests that this is related to errors in the positioning of the Saharan heat low, which is too far south in HadGEM3-RA and associated with an insufficient northward reach of the south-westerly low-level monsoon flow and weaker moisture convergence over the Sahel. Despite these biases HadGEM3-RA's representation of the general rainfall distribution during the WAM appears superior to that of ERA-Interim when using Global Precipitation Climatology Project or Tropical Rain Measurement Mission data as reference. This suggests that the associated dynamical features seen in HadGEM3-RA can complement the physical picture available from ERA-Interim. This approach is supported by the fact that the global HadGEM3 model generates realistic simulations of the WAM without the benefit of pseudo-observational forcing at the lateral boundaries; suggesting that the physical formulation shared with HadGEM3-RA, is able to represent the driving processes. HadGEM3-RA simulations confirm previous findings that the main rainfall peak near 10°N during June–August is maintained by a region of mid-tropospheric ascent located, latitudinally, between the cores of the African Easterly Jet and Tropical Easterly Jet that intensifies around the time of onset. This region of ascent is weaker and located further south near 5°N in the driving ERA-Interim reanalysis, for reasons that may be related to the coarser resolution or the physics of the underlying model, and this is consistent with a less realistic latitudinal rainfall profile than found in the HadGEM3-RA simulations.

1 Introduction

The West African economy and its food supply depend strongly on local agriculture, which is in turn highly dependent on climate, particularly on seasonal rainfall. Rainfall maxima occur during the peak of the West African monsoon (WAM) in June–July–August (JJA) and are associated with the meridional displacement of the intertropical convergence zone (ITCZ). The migration of the ITCZ is not smooth but characterized by successive phases of intense rainfall and pauses (Janicot et al. 2011; Sultan and Janicot 2003). Firstly, the ITCZ holds a quasi-

I. Diallo (✉) · A. T. Gaye · C. Niang · M. D. B. Dieng
Laboratoire de Physique de l'Atmosphère et de l'Océan Siméon
Fongang (LPAO-SF), Ecole Supérieure Polytechnique,
Université Cheikh Anta Diop (ESP-UCAD),
PO Box: 5085, Dakar-Fann, Senegal
e-mail: ismaila1.diallo@ucad.edu.sn; ismailladiallo@gmail.com

C. L. Bain · W. Moufouma-Okia · R. Graham
Met Office Hadley Center, FitzRoy Road, Exeter EX1 3PB, UK

stationary position around the Guinea Coast near 5°N between April and June. Secondly, there is an abrupt shift of rainfall maxima northward to hold another quasi-stationary position near 11°N in JJA. This abrupt latitudinal shift corresponds to the monsoon "onset" and contrasts to the smooth retreat of the ITCZ southward in October–November. Reliable projections of potential changes to the WAM and its onset characteristics are important to inform climate change adaptation in most socio-economic sectors in the region. This paper is concerned with assessing the quality of the HadGEM3-RA simulations of the monsoon; a faithful simulation being evidence that the model has a sound physical basis for use in future projection.

There are disagreements in the literature on the primary dynamical processes influencing the monsoon onset. For instance Sultan and Janicot (2003), using a composite study based on the National Centers for Environmental Prediction (NCEP) reanalysis (Kalnay et al. 1996), argue that interactions between the regional circulation and the Atlas and Hoggar mountains play a critical role in the mechanism leading to the abrupt shift of the ITCZ (defined as the convective rainbelt), through enhancing the Saharan heat low (SHL) cyclonic circulation in the low levels. Gu and Adler (2004) see rainfall maxima along the Guinea coast and Sahelian zone as two independent features, with the former controlled by sea surface temperature (SST) and the latter controlled by upper air atmospheric jets. Okumura and Xie (2004) highlight the influence of SST seasonal cooling in the Gulf of Guinea. Ramel et al. (2006) using the MAR regional climate model have attributed the monsoon onset to an abrupt shift in the SHL position resulting from differences in surface albedo between the Sahel and Sahara desert. Hagos and Cook (2007), also using a regional climate model (RCM), found that the surface sensible heat drives a shallow meridional circulation and moisture convergence at the latitude of the sensible heating maximum, which leads to an inertial instability responsible for the abrupt meridional shift of rainfall maxima. Sijikumar et al. (2006) using the Mesoscale Model MM5 found a deepening of the SHL followed by an enhanced westerly moisture advection from the eastern Atlantic ocean during the WAM onset. This result has been recently consolidated by Vellinga et al. (2013) using the Met Office GloSea4 system, an ensemble prediction system derived from the HadGEM3 coupled ocean general circulation model (GCM). Although climate models can capture reasonably the different phases of the intraseasonal variability of WAM rainfall, the accurate simulation of the onset timing remains a grand challenge and model performance in this respect is very sensitive to physical parameterizations (Hourdin et al. 2010; Sylla et al. 2010a; Yamada et al. 2012; Hernández-Díaz et al. 2013). Flaounas et al. (2012) found for instance that the WAM onset timing of 2006 in WRF regional

climate model simulations is not sensitive to the albedo of the Sahara desert, effects of the North Africa highlands, nor the timing of the SST cold tongue which develops during late spring near the Equator in the Gulf of Guinea; all factors that have been argued as important in other studies.

The purpose of this paper is twofold: (1) explore the performance of HadGEM3-RA, the RCM configuration of the Hadley Centre Global Environmental Model version 3 (HadGEM3; Walters et al. 2011), in simulating features of the WAM onset; (2) use the dynamical fields from the high resolution simulation together with the pseudo-observed fields from the ERA-Interim reanalysis (Dee et al. 2011) to develop hypotheses on the dynamical factors driving the observed features of the monsoon. In this respect, comparisons of the RCM performance against that of HadGEM3, a parent GCM which shares common model components and formulation and which is not forced by pseudo-observed lateral boundaries serve to provide insights on the ability of the model physics formulation to support a realistic monsoon simulation. In Sect. 2 we describe the models, datasets and methodology used. In Sect. 3 we evaluate the models' performance with focus on the spatial distribution of seasonal rainfall total, 2 m air temperature and the annual cycle over selected sub-regions. Potential physical processes controlling the WAM onset in HadGEM3-RA and HadGEM3 simulations are also discussed in this section. A summary and conclusions are provided in Sect. 4.

2 Methodology and evaluation metrics

2.1 Model description and experimental design

The two models used in this study are the Global Atmosphere 3.0 (GA3) configuration of the Hadley Centre Global Environmental Model version 3 (HadGEM3) and its regional climate model version, here referred to as HadGEM3-RA. For a more detailed description of the formulation of both models, the reader is referred to Walters et al. (2011). HadGEM3 is integrated for 27 years (1982–2008) with horizontal grid spacing of $1.875° \times 1.25°$ and 85 model vertical levels, using prescribed daily observed SST/SICE from the Reynolds dataset (Reynolds et al. 2003).

HadGEM3-RA shares common atmospheric and land surface model components with HadGEM3, but is applied over a limited area. The HadGEM3-RA experiment fully complies with the protocol of the Coordinated Regional Climate Downscaling Experiment (CORDEX; Giorgi et al. 2009; http://cordex.dmi.dk/joomla/) over Africa: specifically the model is integrated for 20 years (1989–2008) over the CORDEX whole-Africa domain with atmospheric initial conditions and 6-hourly lateral boundary conditions (LBCs) taken from the European Centre for Medium range
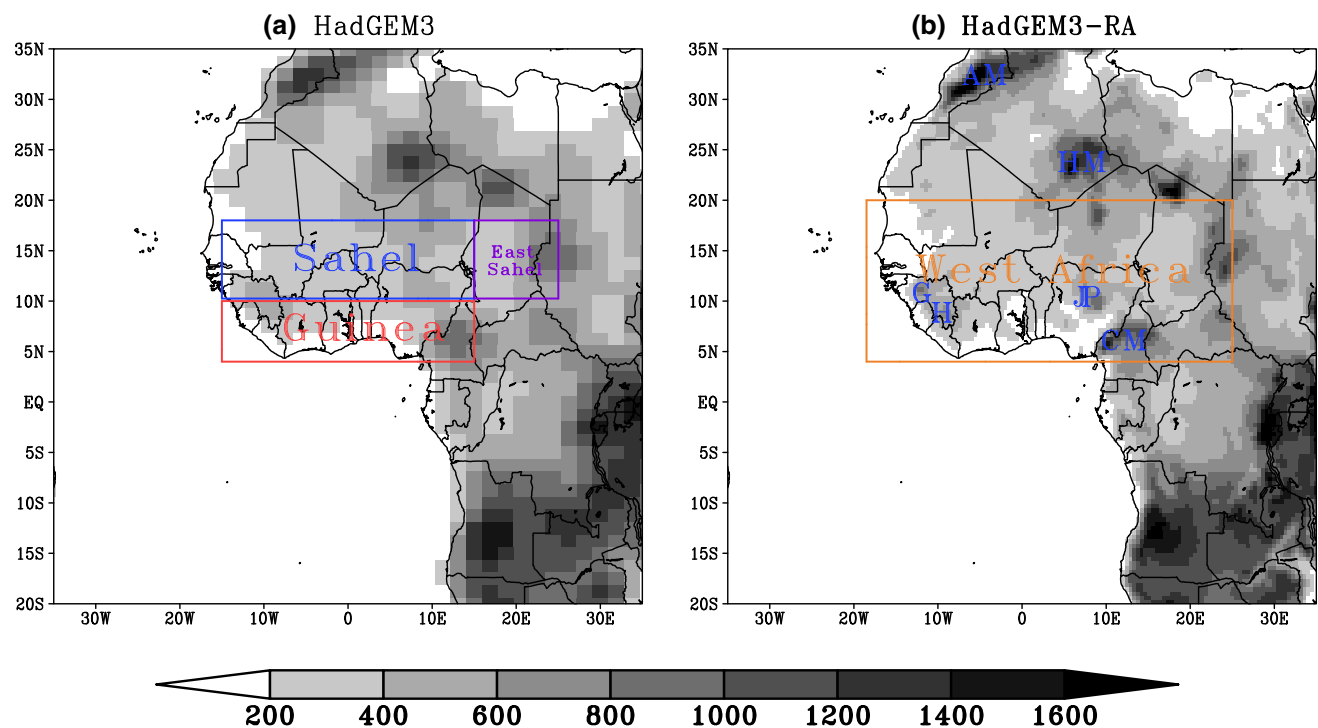
Fig. 1 West African domain topography (in m) from: **a** HadGEM3 and **b** HadGEM3-RA and showing the different sub-regions (Sahel, Guinea, East Sahel and West Africa) and orographic features: *GH* Guinea highlands, *JP* Jos Plateau, *CM* Cameroun Mountains, *AM* Atlas Mountains, *HM* Hoggar Mountains

Weather Forecasting (ECMWF) reanalysis dataset ERA-Interim (Dee et al. 2011) and with a horizontal grid resolution of 0.44° × 0.44°, which roughly corresponds to 50 km on the rotated grid coordinate system. In addition the model employs 63 vertical levels, a time-step of 12-min, and lateral boundary conditions were updated every time-step through a linear interpolation. Reynolds daily observed SST was used to drive the lower boundary conditions of HadGEM3-RA over sea grid-boxes. Since the HadGEM3-RA and HadGEM3 simulations are performed with common SST forcing and number of vertical levels in the troposphere (i.e. below 18 km), differences in the models' behaviour over the Africa domain are attributable to differences in the large-scale driving atmospheric circulations and the impact of resolving smaller scale features in the higher resolution HadGEM3-RA model.

The HadGEM3-RA experiment follows the one-way nesting approach described by Davies (2013). The sponge zone, where the RCM interior flow is gradually relaxed toward the externally imposed lateral flow without feedback to the latter, is set to 10 grid-points and a halo of 5 grid-points is added around the domain edges to provide upstream values for the semi-Lagrangian scheme. The latitude-longitude grid is rotated so that the equator lies always inside the region of interest, in order to obtain a quasi-uniform grid box area throughout the region of interest. Note that no nudging toward the ERA-Interim

LBCs was applied within the HadGEM3-RA domain. The computational domain has 226 × 233 grid-points and was initially designed to include most of the local scale climate drivers, and account for the diversity of climate regimes across Africa.

Figure 1 compares HadGEM3 (Fig. 1a) and HadGEM3-RA (Fig. 1b) topography over West Africa. Both model configurations capture the key regional orographic features including the Guinean Highlands (GH; ∼10.5°N, ∼13°W), Cameroon Mountains (CM; ∼6°N, ∼12.5°E) and Jos plateau (JP; ∼10°N, ∼8°E). However, HadGEM3 lacks fine scale details compared to HadGEM3-RA and this may adversely affect the GCM's ability to simulate rainfall maxima over highland regions.

2.2 Validation data

The validation data used throughout this paper are sourced from the Global Precipitation Climatology Project (GPCP; Huffman et al. 2009), the 3B42-V7 Tropical Rain Measurement Mission (TRMM; Huffman et al. 2007), the ERA-Interim reanalysis (Dee et al. 2011), the Modern-Era Retrospective analysis for Research and Applications (MERRA; Rienecker et al. 2011), the Climatic Research Unit version TS3.0 (CRU; Harris et al. 2012) and the University Delaware observation dataset (UDEL; Legates and Willmott 1990). Use of two observational datasets for both rainfall (GPCP

Table 1 Summary of observational datasets and reanalyses used for the assessment of model results

	CRU	UDEL	GPCPV11	TRMM	ERA-Interim	MERRA
Variables	2 m air temperature	2 m air temperature			2 m air temperature	2 m air temperature
					Rainfall	Rainfall
			Rainfall	Rainfall	Winds	Winds
					Mean sea level pressure	
Spatial resolution	0.5°	0.5°	2.5° for the monthly	0.25°	1.5°	0.5°
			1° for the daily			
Spatial coverage	Land only	Land only	Land/Ocean	Land/Ocean	Land/Ocean	Land/Ocean
Temporal coverage	Monthly; 1990–2007	Monthly; 1990–2007	Monthly; 1979–2009	Monthly; 1998–2007	Monthly; 1990–2007	Monthly; 1990–2007
			Daily; 1998–2009	Daily; 1998–2007	Daily; 1990–2007	Daily; 1990–2007
Data	Observation network	Observation network	Observation network and satellite	Satellite	Model and observations	Model and observations
References	Mitchell and Jones (2005), Harris et al. (2012)	Legates and Willmott (1990)	Adler et al. (2003), Huffman et al. (2009)	Huffman et al. (2007)	Uppala et al. (2008), Dee et al. (2011)	Rienecker et al. (2011)

and TRMM) and temperature (CRU and UDEL) allows some insight into observational uncertainty, given the data scarcity over much of the region. Table 1 provides details of the variables used from each dataset as well as the temporal and spatial resolutions. We have interpolated all the validation datasets and model outputs onto the HadGEM3-RA grid through a bilinear interpolation to facilitate comparisons. We note that ERA-Interim is used both as lateral boundary forcing for the HadGEM3-RA experiment and as one of the validation datasets.

The models' performance is further examined using four sub-regions (Fig. 1), each with different characteristics of the annual cycle of rainfall: Sahel (20°W–15°E; 10°N–20°N), East Sahel (15°E–25°E; 10°N–20°N), Guinea (15°W–15°E; 5°N–10°N), and West Africa (20°W–25°E; 4°N–20°N). The selection of sub-regions is based on the previous work of Moufouma-Okia and Rowell (2010) and three evaluation metrics are used. These include the mean bias (MB), which corresponds to the difference between the area averaged simulated and observed values, the root mean square difference (RMSD), and the pattern correlation coefficient (PCC; i.e. spatial correlation). These metrics are only calculated for rainfall and 2 m air temperature for JJA. GPCP and CRU are used as the main reference datasets for rainfall and 2 m air temperature respectively.

2.3 Onset Index definition

In order to evaluate HadGEM3-RA performance and address the circulation change around the WAM onset date,

an Onset Index (OI) has been defined. This OI is based on the method proposed by Sijikumar et al. (2006) which computes standardized rainfall indices for two regions using the 5-day means of rainfall (hereafter referred to as "pentads") averaged over the region: specifically, a Northern (Sahelian) Index (NI), defined over 10°W–10°E and 7.5°N–20°N and a Southern (Guinean) Index (SI), defined over 10°W–10°E and 0°–7.5°N. We then calculate the difference between the standardized Sahelian and Guinean indices (NI minus SI). Thus a positive (negative) difference indicates that the Sahelian rainfall rate is higher (lower) than the Guinean rate. According to Sijikumar et al. (2006) the onset date is defined as the first pentad for which NI–SI > 0 conditional that the relationship holds for at least the next four pentads (though results for onset timing are similar if this condition on duration is changed to the next two or three pentads).

3 Results and discussions

3.1 Model performance

3.1.1 Precipitation climatology

Figure 2a–f show JJA mean precipitation from, respectively, the GPCP and TRMM observational datasets, the ERA-Interim and MERRA reanalyses and the HadGEM3 and HadGEM3-RA simulations. There is generally good agreement between GPCP and TRMM with major rainfall
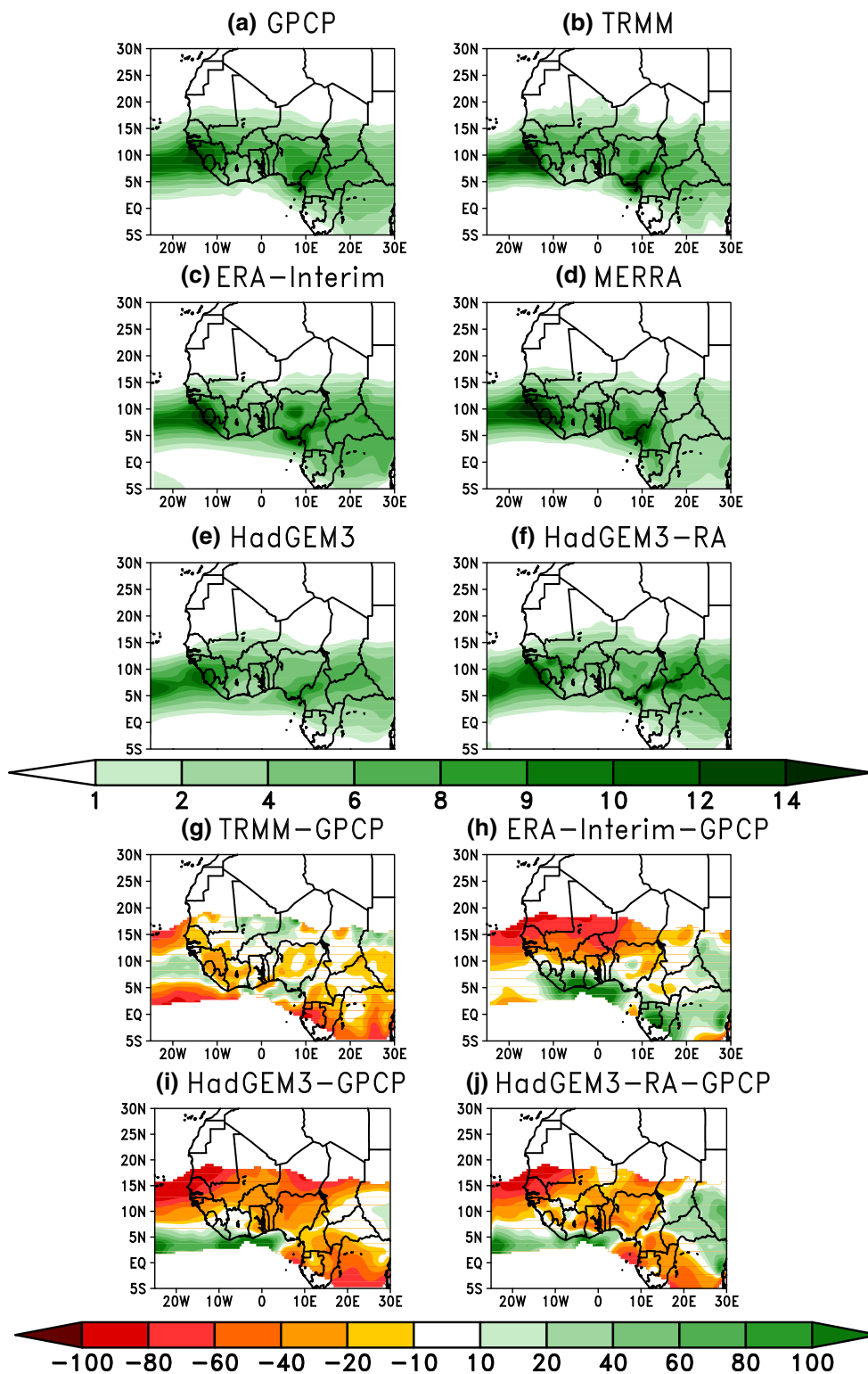
Fig. 2 Mean JJA rainfall (in mm/day) from: **a** GPCP, **b** TRMM, **c** ERA-Interim, **d** MERRA, **e** HadGEM3, **f** HadGEM3-RA and biases with respect to GPCP (expressed in %) from: **g** TRMM, **h** ERA- Interim, **i** HadGEM3 and **j** HadGEM3-RA. The mean is calculated using the 1990–2007 period except for TRMM for which the period 1998–2007 is used

maxima centred over coastal Guinea and along the Nigeria/ Cameroon border and an east–west band of peak rainfall centred near 10°N. TRMM is drier than GPCP along most

Guinea Coast regions and wetter in the central Sahel (Fig. 2g), however broad agreement is reflected in Table 2 which shows differences of no more than 8 % in any of the

Table 2 Mean bias (MB), root mean square difference (RMSD) and the pattern correlation coefficient (PCC) for JJA precipitation for the model simulations (HadGEM3 and HadGEM3-RA), observations (TRMM) and reanalyses (ERA-Interim and MERRA)

	Sahel		East Sahel		Guinea		West Africa		
	Mean bias (%)	RMSD (mm/day)	Mean bias (%)	RMSD (mm/day)	Mean bias (%)	RMSD (mm/day)	Mean bias (%)	RMSD (mm/day)	PCC
TRMM	−4.6	0.65	−7.5	0.47	−4.3	1.33	−5.7	0.83	0.95
ERA-Interim	−27.4	1.29	27.2	0.99	24.1	2.30	6.18	1.51	0.90
MERRA	−24.4	1.25	−32.8	1.09	17.3	2.25	−14.1	1.67	0.86
HadGEM3	−62.6	2.49	−49.3	1.31	−35.1	2.61	−41.1	2.06	0.94
HadGEM3-RA	−17.8	1.09	32.2	1.40	−5.71	1.65	3.31	1.46	0.90

All values are calculated over the 1990–2007 period using GPCP as the reference. The PCC is calculated only for the West African region

sub-regions considered and a pattern correlation of 0.95. The similarity between GPCP and TRMM gives some confidence in their use for model validation. Further, we note that Sylla et al. (2013a) argue that over Africa, GPCP is more consistent with gauge based observations whilst Nikulin et al. (2012) found a significant dry bias over tropical Africa in TRMM compared to GPCP. We therefore select, for precipitation, GPCP as our main observational reference in this paper.

The re-analysis datasets (Fig. 2c, d) show good agreement with GPCP and TRMM with regard to the major maxima and the overall pattern correlation, though less than for TRMM, exceeds 0.86. However the east–west rain band is displaced southward, as is also evidenced in the dipole difference pattern for ERA-Interim (Fig. 2h). This is likely due to the influence of the GCMs in the re-analysis products which, as noted by other authors (e.g. Vellinga et al. 2013), tend to underestimate the northward progression of the monsoon rainband. This positional bias is also evident in Table 2 which shows both ERA-Interim and MERRA to have a dry bias in the Sahel (−27.4 and −24.4 %) respectively) and a wet bias in the Guinea region (24.1 and 17.3 %). These biases and likely corresponding position errors in associated dynamical features are important to keep in mind in subsequent sections where we assess HadGEM3-RA dynamical fields.

With regard to orographic enhancement of rainfall both observations and re-analyses give broadly consistent results over the Cameroon Mountains, while TRMM appears drier than the other datasets in the region of the Guinea Highlands. All four datasets show enhanced rainfall in the region of the Jos plateau (Central Nigeria), with a tendency for a separate peak in TRMM and ERA-Interim; perhaps because of the higher horizontal resolution, though a separate peak is not evident in the (high resolution) MERRA dataset.

Both HadGEM3 and HadGEM3-RA (Fig. 2e, f) produce the main observed rainfall features discussed above: specifically the rainfall peaks near the Guinea Highlands and

Cameroon mountains and the east–west rain band near 10°N. The biases are similar in both models (Fig. 2i, j) with the dominant feature being a dry bias over much of the Sahel and Guinea Coast regions, which is most acute in the Sahel. The broad similarity of the HadGEM3 and Had-GEM3-RA simulations is striking, considering the former is forced by observations only at the lower boundary, and suggests the model physics, common to both models, represents well the physical processes that lead to maintenance of the main rain band near 10°N in JJA. The observed lateral boundary forcing and higher resolution of the HadGEM3-RA simulation are the candidate reasons for its improved simulation relative to HadGEM3, with smaller RMSD and absolute biases in all regions, with the exception of RMSD for East Sahel (Table 2). However, given that the forcing data from ERA-Interim is not consistent with maintenance of a rainband at 10°N, this result suggests that higher model resolution may be the primary reason for the better HadGEM3-RA simulation. The PCC for the whole West Africa region is similar between the two models (slightly lower with HadGEM3-RA). A notable improvement is seen in the Jos plateau region where the rainfall peak observed in GPCP and TRMM is better reproduced in HadGEM3-RA.

In conclusion, although HadGEM3-RA shows some weaknesses, such as a dry bias over much of the Sahel and Guinea Coast region, its performance in replicating the spatial distribution of rainfall appears in line with that documented in previous studies using either RegCM3 (Sylla et al. 2009, 2010b; Diallo et al. 2010; Abiodun et al. 2012) or other state-of-the-science regional climate modelling systems (e.g. Diallo et al. 2012, 2013a, b; Hernández-Díaz et al. 2013; Nikulin et al. 2012; Gbobaniyi et al. 2013; Sylla et al. 2013b).

3.1.2 Temperature climatology

The spatial distribution of the JJA averaged 2 m air temperature is presented in Fig. 3a–d for the four validation
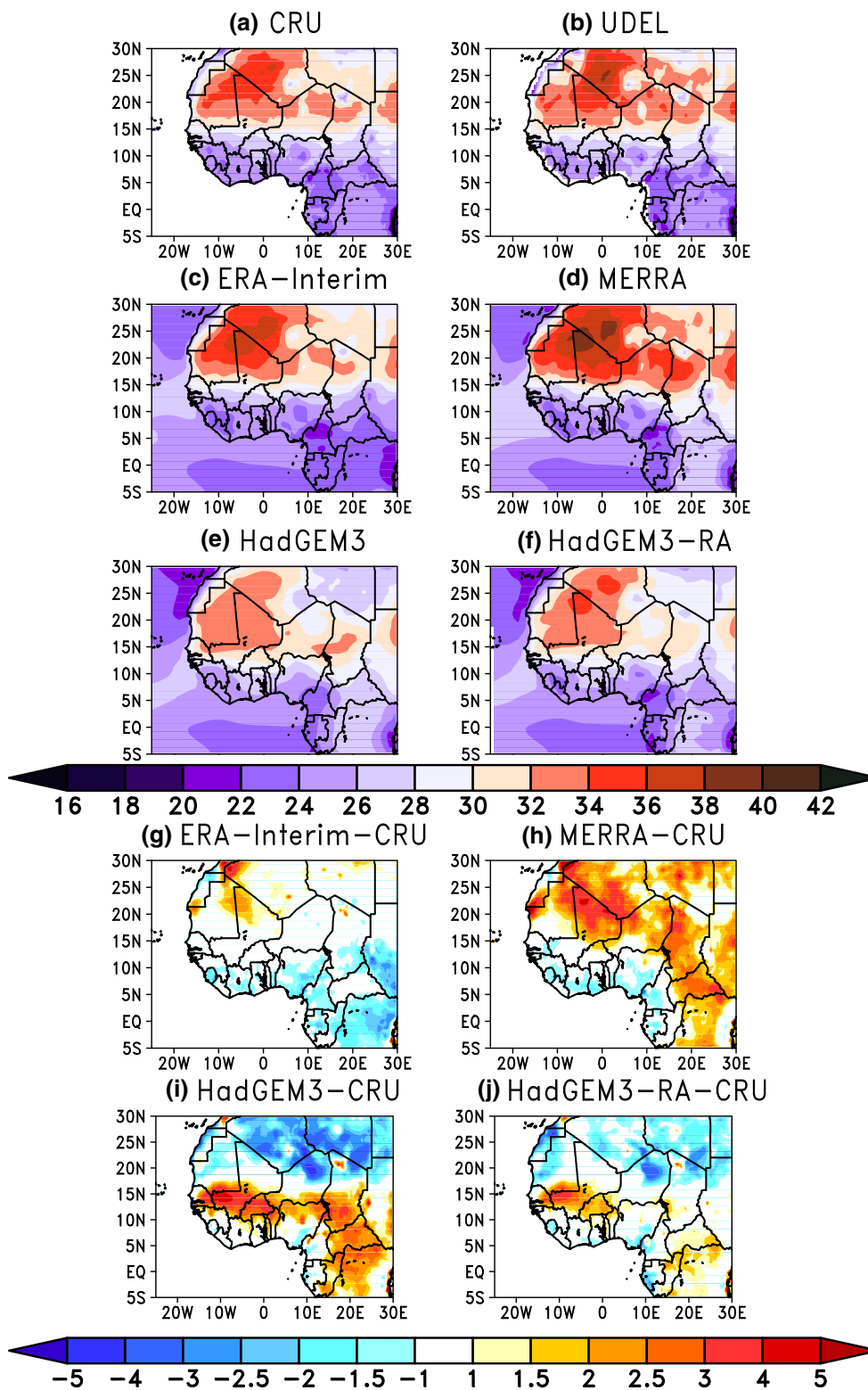
Fig. 3 Mean JJA 2 m air temperature (in °C) from: **a** CRU, **b** UDEL, **c** ERA-Interim, **d** MERRA, **e** HadGEM3, **f** HadGEM3-RA and biases with respect to CRU (expressed in °C) from: **g** ERA-Interim, **h** MERRA, **i** HadGEM3 and **j** HadGEM3-RA. The mean is calculated using the 1990–2007 period

Table 3 Mean bias (MB), root mean square difference (RMSD) and the pattern correlation coefficient (PCC) for JJA mean 2 m air temperature (T2 m) for the model simulations (HadGEM3 and HadGEM3-RA), observations (UDEL) and reanalyses (ERA-Interim and MERRA)

	Sahel		East Sahel		Guinea		West Africa		
	Mean bias (°C)	RMSD (°C)	Mean bias (°C)	RMSD (°C)	Mean bias (°C)	RMSD (°C)	Mean bias (°C)	RMSD (°C)	PCC
UDEL	0.41	0.74	0.51	0.85	−0.14	0.54	0.25	0.75	0.98
ERA-Interim	−0.07	0.52	−0.74	1.01	−1.13	1.03	−0.60	0.91	0.98
MERRA	0.80	1.26	1.70	1.68	−0.97	0.94	0.81	1.41	0.95
HadGEM3	0.71	2.06	0.83	2.19	1.47	1.49	1.08	2.06	0.85
HadGEM3-RA	2.90	2.84	2.32	2.54	0.43	0.89	2.05	2.34	0.91

All values are calculated over the 1990–2007 period using CRU as reference. The PCC is calculated only for the West African region

datasets. CRU locates the main temperature maximum (∼36 °C) in the western Sahara with lowest temperatures (<26 °C) aligned along the Guinea Coast, and with local minima associated with complex terrains such us the Jos plateau, Cameroon mountains and Guinean highlands. The UDEL and reanalysis datasets (Fig. 3b–d) show similarity with CRU in terms of spatial distribution, with PCCs of 0.95 or greater (see Table 3). The reanalysis datasets differ from each other mainly in the magnitude of temperature over the Sahara desert, with MERRA indicating warm biases (relative to CRU) of up to 4 °C. In contrast ERA-Interim shows little bias with respect to CRU (Fig. 3g, h). Over the Guinea Coast, there is consistency between the reanalyses, which indicate patchy cold biases of magnitude up to 2 °C.

The models reproduce well the general features of the observed pattern including the meridional surface temperature gradient between Guinea Coast and the Saharan desert. This temperature gradient is instrumental to the formation and evolution of the African Easterly Jet (AEJ) (Cook 1999; Thorncroft and Blackburn 1999). HadGEM3 and HadGEM3-RA errors are characterized by cold biases over the Sahara, largely over and to the east of the observed 2 m temperature maximum, and warm biases between 10°N and 15°N. For instance, from Table 3 it is seen that while the mean bias (and RMSD) for both models exceeds 2 °C over all sub-regions except Guinea, HadGEM3-RA PCC for West Africa exceeds 0.90. The largest warm biases occur around south-western Mali, east Senegal and Burkina Faso (Fig. 3i, j). These warm biases are consistent with the dry bias found in this region (Fig. 2i, j), as less rainfall would induce less evaporative cooling and increase the insolation through decreased cloud cover.

Another possible explanation for the models' warm biases is further discussed in Garcia-Carreras et al. (2013) whereby a lack of cold pool parameterisation leads to underestimation of heat low ventilation, and a consequent warm bias near the model surface. One effect of the warm

bias is to displace the zone of meridional temperature gradient southward relative to its observed position. It should be noted, though, that all comparisons of temperature at 2 m are affected by large uncertainties due to the relative sparseness of surface observing stations in the region. Overall HadGEM3 and HadGEM3-RA capture the general patterns of observed near-surface temperature, particularly the temperature dipoles, albeit with the noted southward displacement of the zone of meridional gradient.

3.1.3 Wind profile

Figure 4 depicts the vertical cross section of the mean JJA zonal wind averaged between 10°W and 10°E for ERA-Interim, MERRA, HadGEM3 and HadGEM3-RA. The two reanalysis datasets are consistent in their representation of the WAM zonal wind features, including the near-surface westerly component, AEJ in the mid troposphere, and the Tropical Easterly Jet (TEJ) in the upper troposphere. HadGEM3-RA exhibits the same general features of the zonal flow, the main differences from the reanalyses being in the location of the AEJ and the northward limit of the surface westerly flow, both of which are located about 2° south of the position in the reanalyses. Given the large size of the Africa domain, the model is not too constrained over the specific region being considered and the more southerly location is likely a result of the model's physical processes. This is supported by the fact that the HadGEM3 experiment shows a similar more southerly position of the AEJ. Additionally the AEJ is somewhat weaker than seen in the reanalyses while the low-level westerlies are stronger, these differences also seem "inherited" from HadGEM3. The more southerly location of the AEJ in HadGEM3-RA and HadGEM3 is consistent with the more southerly location of the region of zonal temperature gradient (see Fig. 3c–f), as the AEJ is associated with the surface temperature gradient (Cook 1999; Thorncroft and Blackburn 1999). These results suggest that the models' southward
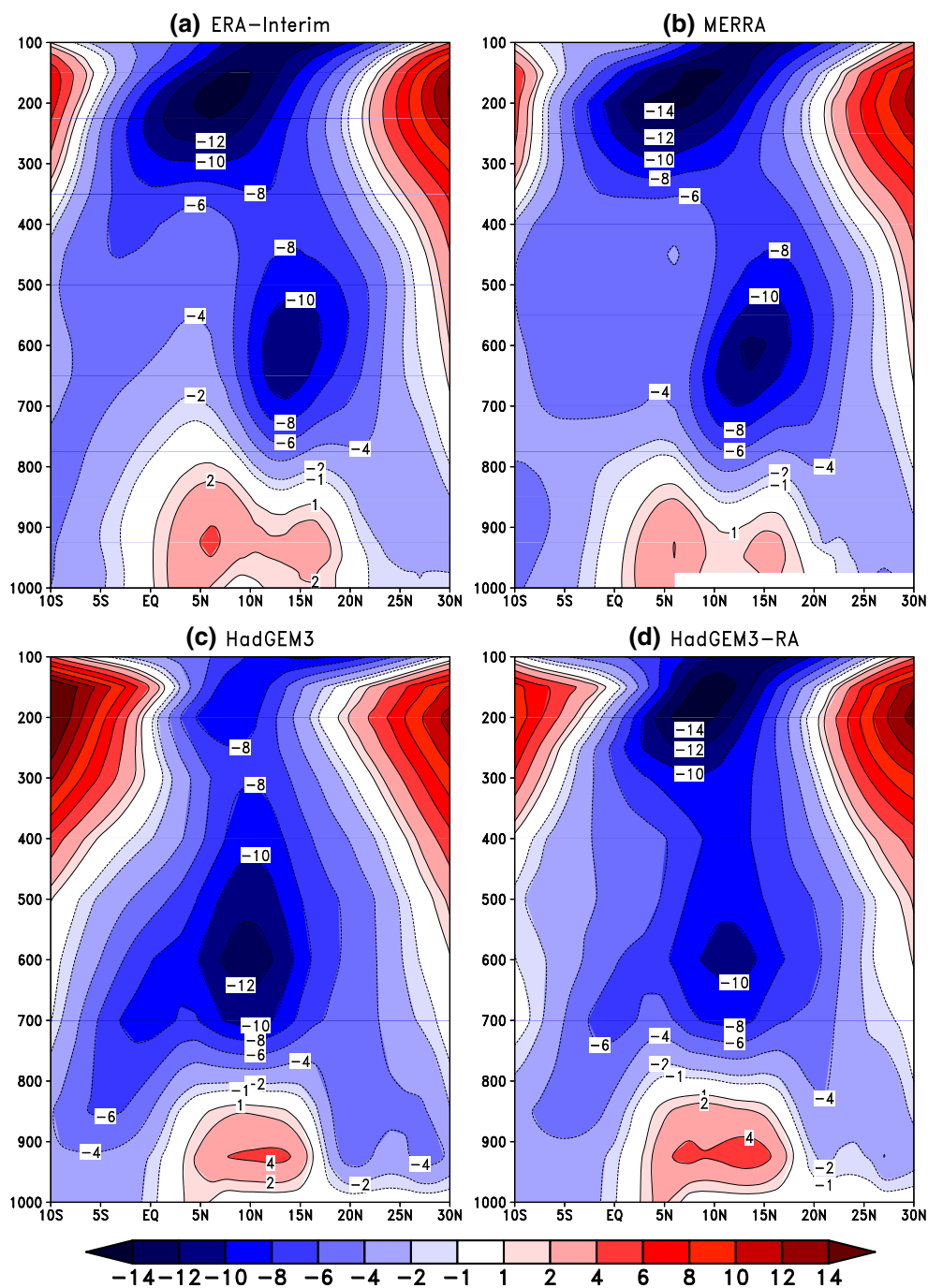
Fig. 4 Vertical cross section of the JJA mean zonal wind (in m/s) averaged between 10°W–10°E from: **a** ERA-Interim, **b** MERRA, **c** HadGEM3 and **d** HadGEM3-RA. The mean is calculated using the 1990–2007 period

shift of the zone of temperature gradient may be associated with a warm bias in the Sahel related to the dry bias, and thus the convection scheme may be implicated. In this context we note that Sylla et al. (2011) concluded that model simulation of the AEJ is sensitive to the convection scheme used. The TEJ (at 200 hPa and 7°N), is very similar in HadGEM3-RA and the reanalyses. In contrast,

the core of the jet is somewhat weaker in HadGEM3 at around 8 m s^{-1} (compared to 14 m s^{-1} in MERRA).

3.1.4 Annual cycle of precipitation

Figure 5 presents the mean annual cycle of rainfall for selected domains shown in Fig. 1. Temporal correlations of
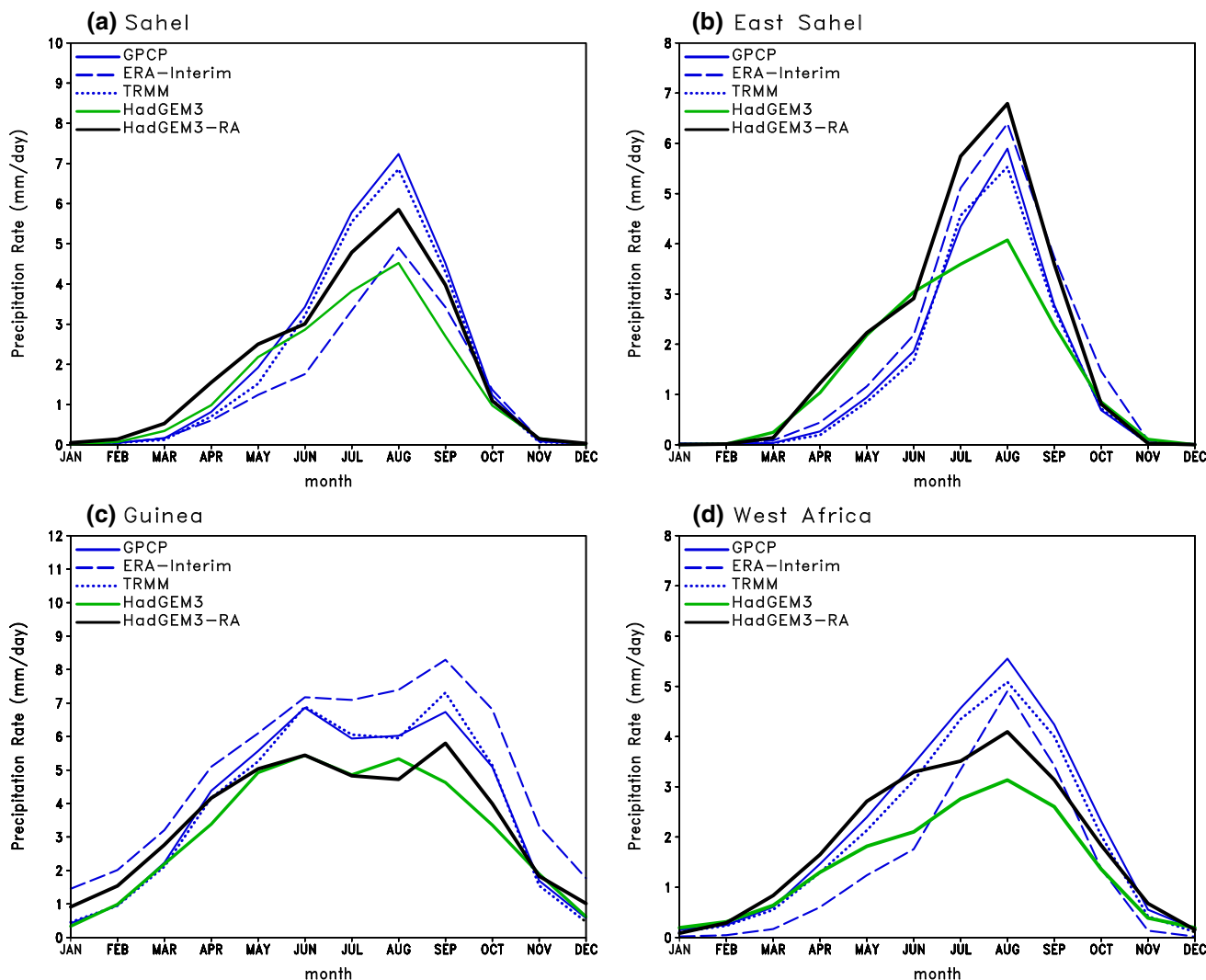
Fig. 5 Mean annual cycle of monthly precipitation (in mm/day) over: **a** the Sahel, **b** the East Sahel, **c** the Guinea region, **d** the West Africa region for GPCP, TRMM, ERA-Interim, HadGEM3-RA and HadGEM3. Means are calculated using the 1990–2007 period except for TRMM for which the 1998–2007 period is used

the annual cycle of monthly rainfall variation for each sub-region, with reference to GPCP, are provided in Table 4. While acknowledging the observational uncertainty, Had-GEM3-RA reproduces fairly well the annual cycle over the main Sahel and East Sahel regions (Fig. 5a, b). The dry season from November to February is well indicated as is the timing of the peak in August, and the subsequent rapid decline. HadGEM3-RA generates too much rainfall in the early season (March to June) particularly in the East Sahel. This bias can be attributed to the model physics, since HadGEM3 which is not constrained by the pseudo-observed lateral boundary input from ERA-Interim exhibits similar behaviour. This similarity is contrasted by the marked departure of the two models after June, including the peak rainfall of August. HadGEM3-RA generates more rainfall than HadGEM3 around the season peak (August)

and is more realistic if we take, as is reasonable, GPCP and TRMM as the most reliable validation. The sudden departure of HadGEM3-RA in this period from the behaviour of HadGEM3 suggests either particular sensi-tivity to the ERA-Interim lateral boundaries at this time or that higher resolution is required to correctly simulate the physical processes developing after onset and at peak rainfall. A similar, though weaker, departure of the two models at this time is also seen in the main Sahel region (Fig. 5a), though here there is less agreement between the observational references; ERA-Interim showing substan-tially less rainfall compared to GPCP and TRMM.

Over the Guinea region (Fig. 5c), GPCP and TRMM show a bimodal distribution of rainfall associated with the meridional progression and retreat of the tropical rain-belt (so called ITCZ) over land. The first rain maximum occurs

Table 4 Temporal correlation coefficients for the annual cycle of sub-region-averaged monthly precipitation for TRMM, ERA-Interim, HadGEM3 and HadGEM3-RA

	TRMM	ERA-Interim	HadGEM3	HadGEM3-RA
Sahel	0.999	0.983	0.978	0.987
East Sahel	0.998	0.993	0.917	0.983
Guinea	0.997	0.984	0.976	0.988
West Africa	0.999	0.974	0.975	0.990

The mean annual cycle is calculated using the 1990–2007 period except for TRMM for which the period 1998–2007 is used. Temporal correlations coefficients are calculated with respect to GPCP

in June and the second one in September with a minima around July–August corresponding to the rainy season over the Sahel. Relative to both GPCP and TRMM, ERA-Interim overestimates rainfall amounts throughout the year, but captures fairly well the timing of rainfall maxima. ERA-Interim overestimation of Guinea region rainfall is in contrast to underestimation in the main Sahel region (Fig. 5a). Rainfall intensities from HadGEM3 and Had-GEM3-RA bear a great deal of resemblance to each other in most of the seasons, which is striking given the lack of pseudo-observational lateral boundary information in HadGEM3 and suggests a dominant role for model physics (over lateral boundary forcing) in the simulated annual cycle. Both models underestimate the rainfall amount compared to ERA-Interim and observations (i.e. GPCP and TRMM). The timing of the highest rainfall amount (June and September) in HadGEM3-RA is in agreement with those of observations and reanalysis. However, HadGEM3 captures only the timing of the first rainfall peak, the second peak occurring too early (in August rather than September). Over the West Africa sub-region (Fig. 5d), we note that both models identify the month of peak rainfall (August) however both, particularly HadGEM3, underestimate the intensity of rainfall over much of the season (relative to TRMM and GPCP).

In summary, the regional model HadGEM3-RA performs notably better than the global model HadGEM3 in simulating rainfall amount and annual cycle over the subdomains, particularly with respect to the peak season amplitude in the Sahel regions and the timing of the rainfall peaks in the Guinea sub-region. This is consistent with the higher correlations for HadGEM3-RA in all sub-regions (Table 4). We have noted some evidence that model resolution plays an important contributing role in this superior performance.

3.2 Intraseasonal variability

In this section we examine the model performance in simulating intraseasonal variability of rainfall and the

abrupt latitudinal shift associated with the monsoon onset. Figure 6a–d show time-latitude diagrams of mean daily rainfall, averaged along 10°W–10°E, from, respectively, GPCP, ERA-Interim, HadGEM3 and HadGEM3-RA. The three phases of the WAM are clearly indicated by GPCP. In the first phase the rainfall maximum remains centred south of 5°N until end of May, after which the rainfall rate diminishes before increasing rainfall rates emerge near and north of 10°N, signifying the start of the rainy season over Sahel (the second phase), with highest rainfall rates occurring during August. In the third phase, from August to October, GPCP shows a southward retreat of the main rainband corresponding to the second rainy season over the Guinean region. The ERA-Interim reanalysis reproduces the general features seen in the GPCP data, but there are important differences. Specifically, rainfall lingers too long over the Guinea Coast with the northward "jump" of the rainfall band occurring too late (early July), the rainband does not move sufficiently far north; with the region of peak rainfall staying south of 10°N, and the rainfall intensities are generally higher than in GPCP. The southward bias in the position of the rainband may be associated with corresponding errors in the representation of dynamical processes supporting the rainfall. Apart from the higher rainfall intensities the relatively smooth southward retreat of rainfall after August is well captured.

HadGEM3-RA (Fig. 6d) simulates the evolution of the position of the tropical rainbelt well. In the first phase, rainfall intensities over the Guinea Coast are similar to GPCP and decrease at the end of May as observed. The northward jump of the rainfall band occurs with similar timing to that of GPCP with peak rainfall in August as observed; though the intensities are lower than in GPCP. The southward retreat of rainfall between August and September is also well simulated. Thus the HadGEM3-RA timing of the onset of rains in the Sahel and the positioning of the rainfall band north of 10°N after the discontinuous "jump" fit better with GPCP than does the ERA-Interim reanalysis. This suggests that the HadGEM3-RA simulation in this region is not dominated by the ERA-Interim boundary forcing and that the model physics and/or high resolution are responsible for the good simulation. This is supported by the HadGEM3 simulation which, although not forced with any pseudo-observed lateral boundary data, bears general similarity to the HadGEM3-RA simulation, particularly with regard to the decreasing Guinea rainfall at the end of May, the northward "jump" in mid-June and the penetration of the rainfall maxima north of 10°N (albeit with intensities that are too low). This similarity indicates that the model physics is critical for realistic positioning of the rainband while high resolution may be more important for attaining realistic rainfall intensities.
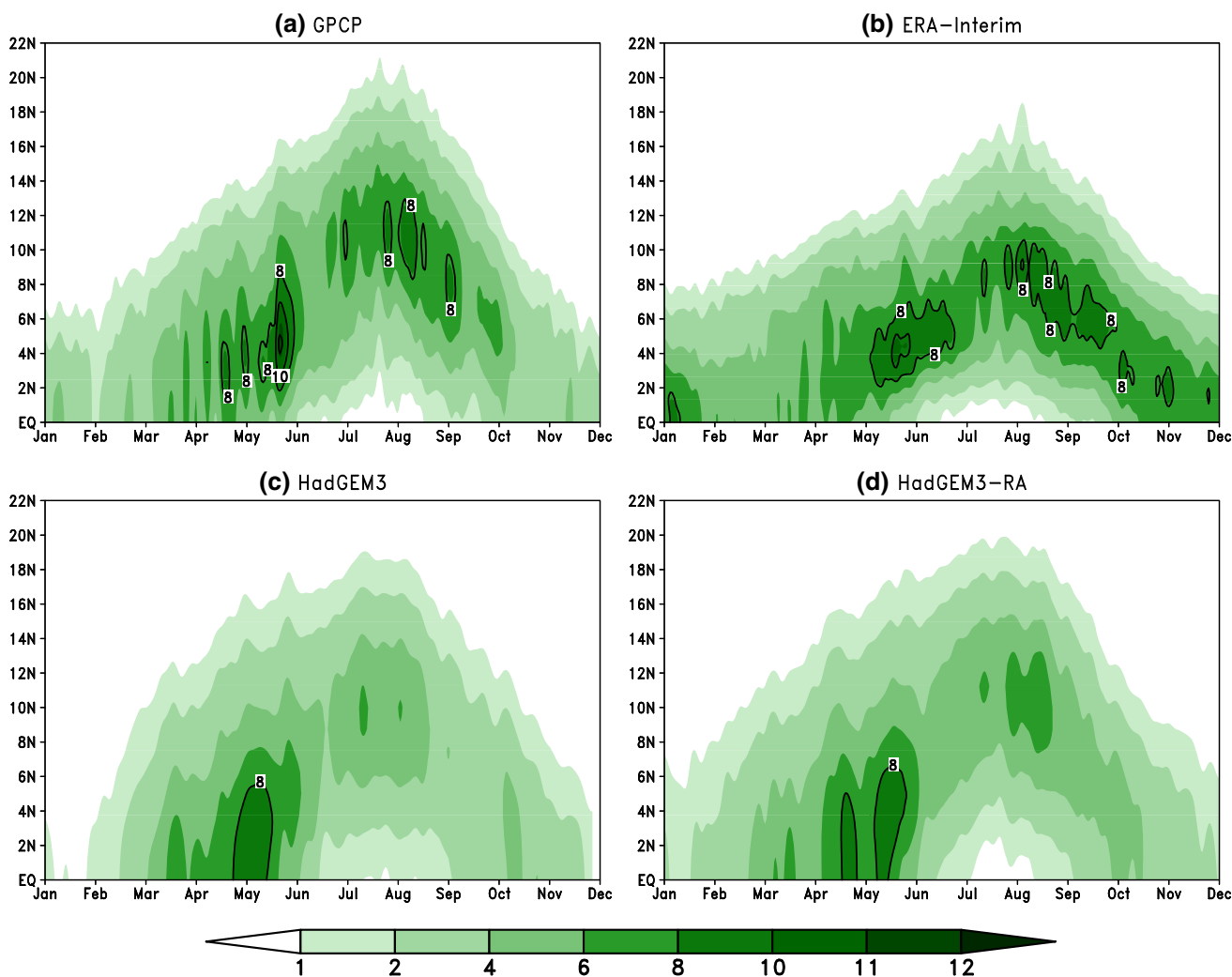
Fig. 6 Time latitude diagram of daily mean precipitation (in mm/day) averaged along 10°W–10°E from: **a** GPCP, **b** ERA-Interim, **c** HadGEM3 and **d** HadGEM3-RA. Means are calculated using the 1990–2007 period

The main driving force of the ITCZ propagation northward over land is the low-level meridional flow (between the surface and 800 hPa) and the AEJ at 600–700 hPa height in association with the intense solar heating over the Sahara (Sultan and Janicot 2003; Yamada et al. 2012; Thorncroft et al. 2011). Figure 7 shows time/latitude diagrams of mean low-level (925 hPa) wind divergence (Fig. 7a–c) and 700 hPa relative vorticity (Fig. 7d–f) averaged along 10°W–10°E. Here, negative (positive) values denote convergence (divergence) while positive (negative) vorticity values correspond to cyclonic (anticyclonic) circulation. From April to early June, ERA-Interim (Fig. 7a) shows strong convergence associated with the leading edge of the northward moving low-level westerlies. The peak divergence is located north of the band of peak rainfall (Fig. 6b) and reaches around 16°N in August before retreating southward. Until June/July a band

of divergence is found to the south of the convergence zone. This is interrupted after July as a further region of divergence develops between 8°N and 10°N, south of the main divergence band. This secondary area of divergence is co-located with the latitude of peak ERA-Interim rainfall after the northward jump (Fig. 6b). Over the Guinea Coast a region of weak convergence is seen south of 4°N until June when it is replaced by divergence; this is consistent with rainfall in that region and its decrease in late June (Fig. 6b).

The general features of the ERA-Interim 925 hPa divergence are well reproduced by both HadGEM3 and HadGEM3-RA, indicating that the model is not dependent on pseudo-observational lateral boundary information to simulate the evolution of the divergence field. The secondary area of convergence that develops between 8 and 10°N around the time of onset in the Sahel is also
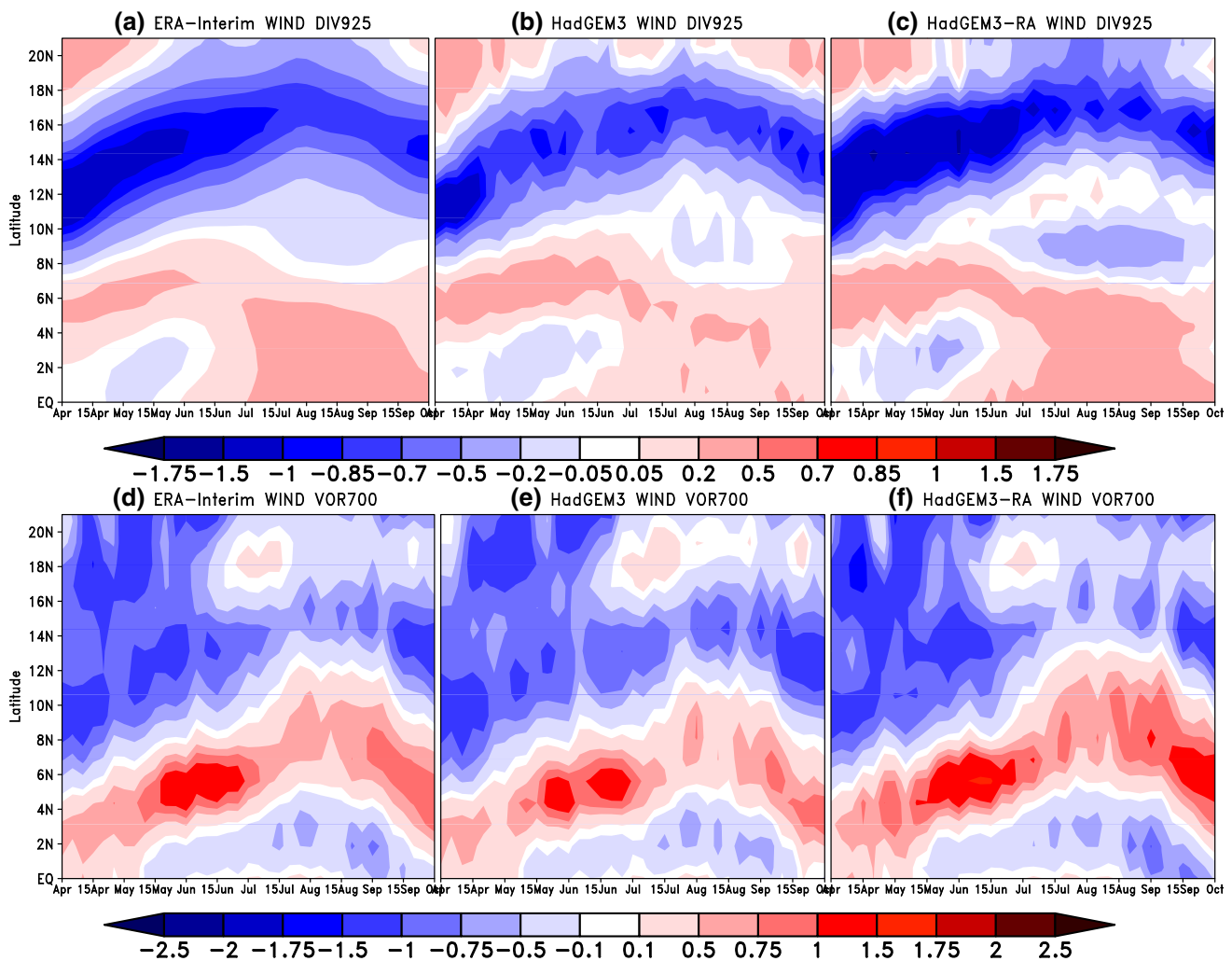
Fig. 7 Time latitude diagram of mean 925 hPa wind divergence (*top panels* l/s) and 700 hPa relative vorticity (*bottom panels* l/s) averaged along 10°W–10°E for: **a**, **d** ERA-Interim, **b**, **e** HadGEM3, **c**, **f** HadGEM3-RA. Means are calculated using the 1990–2007 period. In the *upper panels*, values are multiplied by 10^6 while in the *lower panels*, values are multiplied by 10^5

reproduced by both models, but is much more pronounced in HadGEM3-RA in which it appears separated from the northern region of divergence associated with the leading edge of the low-level westerly flow. Because of the scarcity of radiosonde wind observations in this region, it is not possible to conduct an independent assessment of the realism of the ERA-Interim, HadGEM3 and HadGEM3-RA divergence fields. However, given HadGEM3-RA's superior representation of the northerly jump of the rainband relative to ERA-Interim (Fig. 6), it seems reasonable to assume that the dynamical features generated by HadGEM3-RA can give additional insight to the WAM processes in addition to the pseudo-observational fields from the reanalyses.

Figure 7d–f provide time-latitude diagrams of mean 700 hPa relative vorticity averaged along 10°W–10°E. ERA-Interim, HadGEM3 and HadGEM3-RA all show a region of positive relative vorticity that remains co-located with the main rain band (Fig. 6) as it moves northward. The northward jump also manifests itself in the vorticity field. Consistent with the rainfall results, HadGEM3-RA generates the largest northward shift in the vorticity maximum, which it maintains at a position near 9°N during July and August after which it retreats southward. HadGEM3-RA also has the largest vorticity values. Reference to the JJA vertical cross-section of zonal flow (Fig. 4) shows that the vorticity maximum is associated with sheared easterly flow on the southern side of the AEJ.

To summarise, HadGEM3-RA has a good simulation of the rainfall evolution of the WAM and generates a realistic northward shift of the rainband associated with the onset of the rainy season in the Sahel. Caution must be exercised when using ERA-Interim to assess the evolution of dynamical features, since ERA-Interim has a less realistic

Fig. 8 Standardized difference between the northern (Sahelian) rainfall index (NI; 10°W–10°E; 7.5°N–20°N) and the southern (Guinean) rainfall index (SI; 10°W–10°E; 0–7.5°N) for the period 1998–2007 for: GPCP (*blue line*), ERA-Interim (*green line*) and HadGEM3-RA (*black line*)
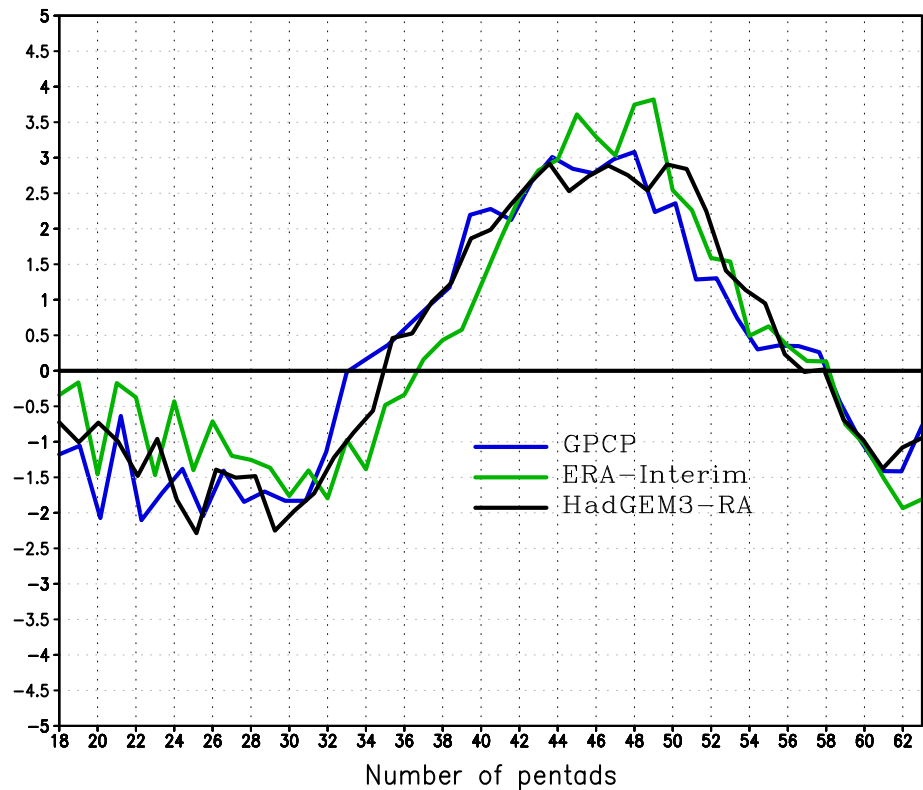

representation of the northward jump. However, Had-GEM3-RA fields of vorticity and divergence are consistent with observed rainfall evolution and are not inconsistent with those observed in ERA-Interim. Of particular interest are the regions of 925 hPa convergence that develops between 8 and 10°N after June and appears associated with the shift of rainfall into the Sahel. It is noteworthy that the broad features of HadGEM3-RA simulation are well reflected, albeit with less detail, in the HadGEM3 simulation. This suggests that HadGEM3-RA is not dependent on pseudo-observed lateral boundary conditions from ERA-Interim for the realism of the simulation, and that the model physics is the most important factor.

3.3 Monsoon onset

In this section we employ the objective measure of onset timing described in Sect. 2.3 to complement the analysis of the previous section. Figure 8 presents the mean onset date computed for the 10 year period 1998–2007 for GPCP, ERA-Interim reanalyses and HadGEM3-RA. By this definition, the mean onset date in the HadGEM3-RA simulations falls in the 35th pentad (21–25 June) two pentads after mean onset in GPCP (33rd pentad; 11–15 June), indicating a bias to late onset timing. Confirming the results shown in Fig. 6, mean onset in ERA-Interim occurs later than in HadGEM3-RA in the 37th pentad (01–05

July). Overall the onset date in HadGEM3-RA compares adequately with the mean onset date from station data over Sahel, i.e. June 24th (Sultan and Janicot 2003; Drobinski et al. 2009); supporting the notion that onset timing in ERA-Interim has a more severe late bias than HadGEM3-RA.

To better understand the HadGEM3-RA behaviour and the dynamical process surrounding the onset date, we next analyse the mean differences between variables averaged over the four pentads after the onset date and over the four pentads before the onset date, using the onset timings referred to above. The variables considered are zonal wind, meridional wind, 2 m air temperature, mean sea level pressure, specific humidity and vertical wind. Figure 9a, b show the low-level (925 hPa) wind differences (arrows) superimposed over the 2 m air temperature differences (shading) and the mean sea level pressure differences (contours) from ERA-Interim and HadGEM3-RA. Both ERA-Interim and HadGEM3-RA show an increase in westerly flow both over the Guinea region and between 12 and 20°N, the latter increase being associated with an increased north–south pressure gradient due to the intensifying heat low. The increased flow from the Atlantic is associated with increased moisture advection into the Sahel (see e.g. Vellinga et al. 2013) a prerequisite for generating rainfall in this region after onset. Vellinga et al. (2013) note that the strong deepening of the heat low in the western
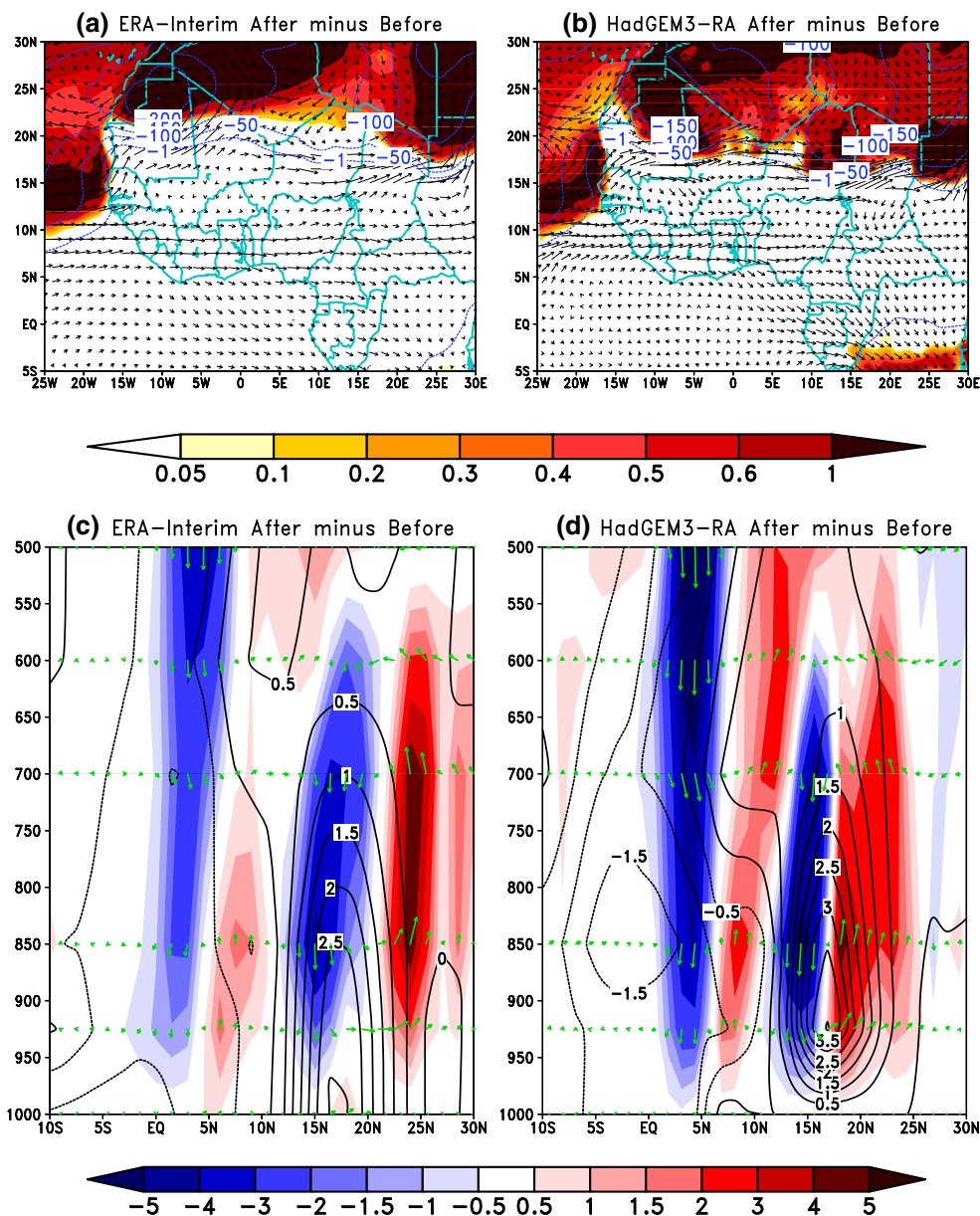
Fig. 9 **a**, **b** Difference between 10-year (1998–2007) means averaged over the four pentads after the onset and the four pentads before the onset. Variables shown are 925 hPa wind (*arrows* m/s), mean sea level pressure (*contours* hPa) and 2 m air temperature (*shading* °C) for: **a** ERA-Interim, and **b** HadGEM3-RA. **c**, **d** As **a**, **b** but for north–south vertical cross sections of averages along 10°W–10°E for mean vertical velocity (*shading* mm/s), specific humidity (*contours* g/kg) and vertical circulation (*arrows* m/s, combining vertical (mm/s) and meridional velocity components (m/s) for: **c** ERA-Interim and **d** HadGEM3-RA

Sahara in ERA-Interim generates increased southerly flow (seen centred near 5°W in Fig. 9a) which may divert moisture north of the Sahel and into the Sahara. In contrast HadGEM3-RA has a more pronounced zonal component in flow difference; suggesting greater eastward moisture flow along the length of the Sahel region. This may be a contributing factor in the smaller dry bias in the Sahel region in HadGEM3-RA relative to ERA-Interim (see Table 2).

Figure 9c, d show vertical cross-sections (10°S–30°N) of differences ("after" minus "before" onset) in vertical velocity (shading), specific humidity (contours) and vertical circulation (arrows; showing a combination of vertical and meridional velocity components). ERA-Interim shows a region of increased vertical motion centred near 24°N extending to around 600 hPa with a region of increased descent of similar depth to its south near 15°N. These features appear to correspond to a strengthening of the shallow meridional circulation cell (SMC) from the surface to the mid-troposphere (Nicholson 2009a; Thorncroft et al. 2011; Sylla et al. 2011) the ascending branch of which lies

about 7 degrees poleward of the rainfall maximum (Nicholson [2013]) and is associated with the low-level convergence of the south-westerly monsoon flow and northeasterly Harmattan winds. The increased meridional circulation is also evident in the HadGEM3-RA simulations (Fig. 9d) with similar vertical extent though with a slight southward displacement. A column of increased moisture centred near 17°N is associated with the SMC in both ERA-Interim and HadGEM3-RA. At low-levels this increased moisture appears associated with the increased westerly flow from the Atlantic evident in Fig. 9a, b. A shallow region of increased ascent following onset is also seen in ERA-Interim near 5°N which may correspond to increased ascent generated by an increase in frictional induced convergence in the southwesterly flow at the interface of the Gulf of Guinea and the West African coast (Nicholson [2008], [2009b]). A similar feature with an ascent maximum also at 850 hPa is also evident in HadGEM3-RA but is further north and much deeper in extent and thus less evidently driven by surface effects. The major difference between HadGEM3-RA and ERA-Interim changes before and after onset is the region of increased vertical ascent in HadGEM3-RA located between 10°N and 12°N above 750 hPa. This region of increased vertical motion is almost entirely absent from ERA-Interim. Although most marked above 750 hPa in HadGEM3-RA, this region of increased ascent extends to low-levels and appears associated with the secondary region of increasing low-level convergence that develops near this latitude around the time of onset (Fig. 7c). This secondary convergence zone also develops in ERA-Interim but is less pronounced. South of these features a region of increased descending motion is seen in both ERA-Interim and HadGEM3-RA between the equator and 5°N and is associated with surface divergence that dominates in that region after onset (Fig. 7a, c).

We now investigate how the changes to the vertical motion field during the onset period relate to the vertical motion patterns seen during the peak of the monsoon season (JJA) and how these are related to the meridional distribution of precipitation. Figure 10a, b show the vertical cross-section of mean JJA vertical velocity (shading) and vertical circulation (arrows) for ERA-Interim and HadGEM3-RA respectively. For cross reference the meridional distribution of precipitation from TRMM, ERA-Interim and GPCP is shown in Fig. 10c while that for HadGEM3-RA and again TRMM and GPCP is shown in Fig. 10d. We note that the TRMM data (Figs. 10c, d) shows two rainfall peaks: a primary peak at 10°N and a secondary peak at 5°N. It is evident from Fig. 10b that the region of increased ascent near 10°N after onset in HadGEM3-RA (Fig. 9d) is maintained through the peak season and is associated with a rainfall peak at 10°N (Fig. 10d) which closely matches the location of the

observed peak in the TRMM dataset (see Fig. 10c). This area of ascent is not matched as a separate feature in the ERA-Interim reanalysis; instead the ascent at this latitude at upper levels appears merged with the low-level ascent due to frictional processes, resulting in over emphasis, relative to TRMM, of the rainfall peak at 5°N. In terms of temporal evolution, ERA-Interim's over emphasis of the JJA rainfall peak near 5°N is related to its delay of the main rainfall band over the Guinea Coast region until late June (Fig. 6b), and comparison of the ERA-Interim and HadGEM3-RA vertical velocity fields (Fig. 10a, b) suggests this may in turn be associated with a late or too weak development of ascent near 10°N. In HadGEM3-RA, in contrast to ERA-Interim, the ascent associated with frictional processes near 5°N is a shallow feature, disconnected from the ascent near 10°N, and associated with a secondary weaker rainfall peak (as observed). Both ERA-Interim and HadGEM3-RA exhibit a broad region of vertical ascent north of 15°N that is associated with smaller rainfall amounts in that region. This area of area of ascent has a double structure and stretches north to 25°N with peak values between 850 and 700 hPa. This region of ascent is associated with the low-level convergence zone at the northern edge of the low-level southwesterly flow (Fig. 7a, c) and lays well north of the rainfall maximum (Fig. 10c) suggesting that the convergence zone (ITCZ) is decoupled from the rainfall maxima. Similar conclusions were drawn by Nicholson ([2009b]).

To summarise the findings of this section HadGEM3-RA is found to develop increased ascent near 10°N, and largely above 750 hPa, during the period of rainfall onset in the Sahel that is not matched in the ERA-Interim dataset. The region of ascent is maintained as a distinct feature through the JJA period and is associated with a rainfall peak at 10°N, the position and intensity of which verifies well with TRMM data. These results support the findings of Nicholson ([2008]) who also relate the rainfall peak to a region of ascent bounded, latitudinally, by the cores of the AEJ and TEJ and also those of Sylla et al. ([2010a]) who draw similar conclusions from simulations with the RegCM3 RCM. A shallow region of ascent near 5°N is associated with a secondary rainfall peak which also verifies well with TRMM data. This shallow ascent, which has been associated with frictional convergence at the West African coast, is also present and is much stronger in ERA-Interim; a fact which appears connected to a late and less marked move of the main rainband north of the Guinea Coast and a consequent overestimation of the secondary rainfall peak. Both ERA-Interim and HadGEM3-RA show a double structured region of ascent maxima to the north of the rainfall maximum which appear broadly related to convergence at the leading edge of the low-level southwesterlies.
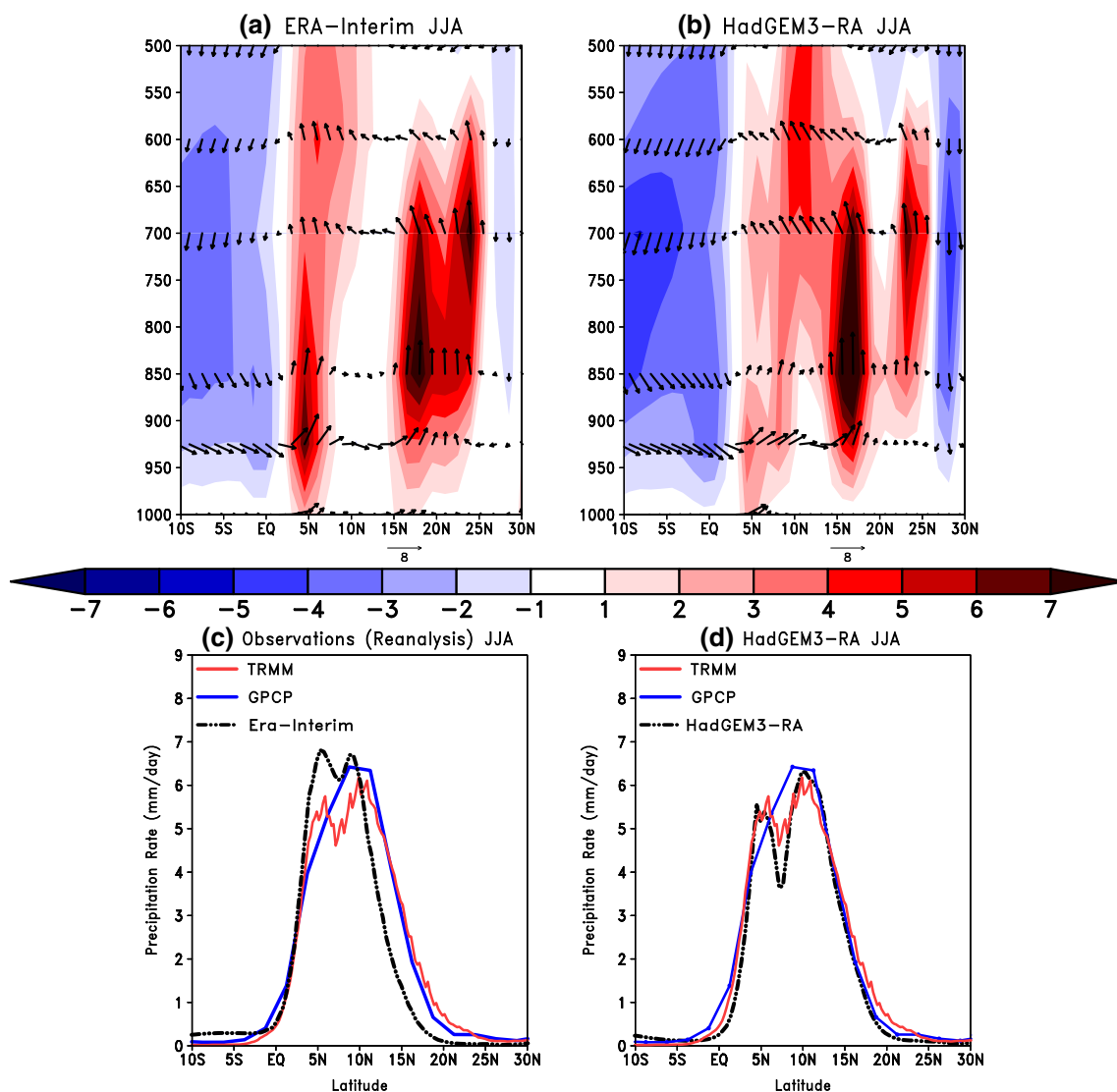
Fig. 10 a, b Vertical cross-sections of mean JJA vertical velocity (*shading* mm/s), specific humidity (*contours* g/kg) and vertical circulation (*arrows* m/s, combining vertical (mm/s) and meridional velocity components (m/s) for: **a** ERA-Interim and **b** HadGEM3-RA. **c, d** north–south profile of mean JJA precipitation (mm/day) for: **c** observations (i.e. TRMM and GPCP) and re-analysis (ERA-Interim) and **d** HadGEM3-RA including TRMM and GPCP. All quantities are averaged along 10°W–10°E and for the period 1990–2007, except for TRMM which is averaged for the period 1998–2007

4 Summary and conclusions

Improving the understanding and predictability of the WAM is of high importance for the Sudano-Sahelian countries, whose economies are mainly based on rain-fed agriculture and therefore vulnerable to climate variability. In this study we have evaluated simulations generated by the HadGEM3-RA RCM and used these simulations, together with ERA-Interim reanalysis data to investigate the dynamics behind the characteristic rainfall evolution, including the discontinuous northward jump of the rain-band in late June that signals the onset of the rains in the Sahel region. HadGEM3-RA was configured over the CORDEX whole-Africa domain, using a horizontal grid spacing of 0.44° (∼50 km), and driven by the ERA-Interim reanalysis for the period 1989–2008.

It is found that, for the peak JJA season, HadGEM3-RA simulates the spatial patterns of rainfall and 2 m temperature well, though with a number of biases. For rainfall, the main observed peak near 10°–11°N is reproduced but there is a widespread dry bias which is most acute in the Sahel region. However, biases are generally smaller in magnitude than in corresponding fields from the forcing ERA-Interim dataset and it is notable that the position of the rainfall peak is more realistic in HadGEM3-RA than in ERA-Interim when compared to GPCP and TRMM

data. For temperature HadGEM3-RA has a widespread cold bias in and to the east of the region of highest temperature over the Sahara and a warm bias between 10°N and 15°N, the latter being possibly linked to increased insolation due to less simulated cloud and rainfall. This warm bias results in the positioning of the region of marked south-north temperature gradient between the Sahara and Guinea coast too far south. Key features in the low-, medium- and upper-level zonal winds are also well simulated including the low-level westerly monsoon flow and the AEJ, though the northerly extent of the westerly flow and the latitudinal position of the AEJ are each located about 2° south of their position in reanalysis data. The latter error being consistent with the displaced zone of 2 m temperature gradient. Associated southerly displacement errors in low-level moisture inflow and dynamics associated with AEJ are likely contributors to the maximum in the dry bias over the Sahel.

It is notable that global model simulations with Had-GEM3, which shares a common model formulation with HadGEM3-RA and identical SST boundary forcing, are of comparable quality, in many aspects, to those of Had-GEM3-RA despite their lack of constraint with pseudo-observed lateral boundary forcing. This suggests that the model physics in both systems has a good ability to represent the processes that sustain the large scale features of the WAM circulation. However, HadGEM3-RA simulations are superior to those of HadGEM3 in generating the peak rainfall in August in the Sahel; suggesting that smaller scale processes may increase in importance during this phase of the WAM, with simulation benefiting from higher resolution.

The time evolution of HadGEM3-RA rainfall matches well the observed evolution, including the timing of the discontinuous northward jump of the main rainfall band in late June, which occurs two pentads later than in GPCP. The simulation also reproduces the position of the maximum rainfall north of 10°N as observed, though the rainfall intensities in the peak month of August are too weak. The HadGEM3-RA evolution is superior to that of ERA-Interim, which has the northward jump 4 pentads later than GPCP and has insufficient northward travel in the main rainband. The superiority of HadGEM3-RA's representation and the fact that the broad features are well reproduced by HadGEM3 again suggest that the degree of realism in these aspects in the HadGEM3-RA simulation derives chiefly from the model physics rather than the pseudo-observed boundary data.

Investigations of changes in the underlying dynamics across the time of onset indicate that ahead of onset a region of low-level divergence which trails a region of convergence associated with the leading edge of the southwesterly flow is eroded by development of a secondary region of convergence between 8°N and 10°N. This feature develops in ERA-Interim, HadGEM3 and HadGEM3-RA but is most developed in the latter. Associated with this developing region of convergence there is, in HadGEM3-RA, a marked increase in ascent near 10°N which peaks between 700 and 500 hPa. This column of ascending air is maintained as a distinct feature through the JJA period, located between the latitudes of the AEJ and TEJ and is associated with a primary rainfall peak near 10°N, as observed in the TRMM data; results that support those of Nicholson (2008) and Sylla et al. (2010a). It is located south of a stronger, lower level area of ascent, near 16°N, associated with convergence at the leading edge of the low-level southwesterly flow which is associated with lower rainfall amounts. A secondary rainfall peak is also generated near 5°N, as observed in TRMM, and appears related to previously suggested (Nicholson 2008) frictional convergence in the southwesterlies at the Guinea Coast. It is notable that although ERA-Interim also has the region of ascent near 16°N, it does not exhibit an increase in ascending motion near 10°N during onset and ascending motion during JJA does not appear at this latitude as a separate column. Weaker ascent is seen further south where it merges with the lower level (frictionally forced) ascent near 5°N. This appears to result in an erosion of the main (10°N) rainband in ERA-Interim and overemphasis of the maxima near 5°N; biases in the JJA mean that are also consistent with the late (end of June) northward jump of the rainband.

Thus the realism of the HadGEM3-RA rainfall simulations, supported by broadly similar simulations from HadGEM3, suggests that the high resolution runs may be used to help diagnose the underlying dynamics. Results suggest that the main rainfall peak in the Sahel in JJA is supported by ascending motion, generated by relatively small scale dynamical features, that increases in intensity near 10°N around the time of onset. Further research is needed to investigate the dynamical origin of this ascending motion. We are also able to tentatively diagnose errors in the latitudinal distribution of ERA-Interim rainfall as being likely due to a failure to support sufficient vertical motion in the region between the cores of the TEJ and AEJ, perhaps because of insufficient resolution in the underlying reanalysis model.

Our analyses show that in simulations of past climate, forced with pseudo-observed boundary data, HadGEM3-RA is capable of providing a realistic representation of the seasonal evolution of precipitation, 2 m air temperature and the associated circulation patterns as well as intraseasonal variability over West Africa. The results provide a useful foundation for interpretation of future work in which HadGEM3-RA will be used to downscale GCM simulations of past climate and future projections.

References

Abiodun BJ, Adeyewa ZD, Oguntunde PG, Salami AT, Ajayi VO (2012) Modeling the impacts of reforestation on future climate in West Africa. Theor Appl Climatol. doi:10.1007/s00704-012-0614-1

Adler RF et al (2003) The version-2 Global Precipitation Climatology Project (GPCP) monthly precipitation analysis (1979–present). J Hydrometeorol 4(6):1147–1167

Cook KH (1999) Generation of the African easterly jet and its role in determining West African precipitation. J Clim 12:1165–1184

Davies T (2013) Lateral boundary conditions for limited area models. Q J R Meteorol Soc doi:10.1002/qj.2127

Dee DP et al (2011) The ERA-Interim reanalysis: configuration and performance of the data assimilation system. Q J R Meteorol Soc 137:553–597. doi:10.1002/qj.828

Diallo I, Camara M, Sylla MB, Gaye AT (2010) Représentation haute résolution du système de mousson Ouest Africain avec un modèle climatique régional. Journal des Sciences Pour l'Ingénieur No 12:75–85. Disponible sur http://www.ajol.info/index.php/jspi/article/viewFile/67978/56073

Diallo I, Sylla MB, Giorgi F, Gaye AT, Camara M (2012) Multi-model GCM-RCM ensemble based projections of temperature and precipitation over West Africa for the early 21st century. Int J Geophys, 2012, Article ID 972896. doi:10.1155/2012/972896

Diallo I, Sylla MB, Camara M, Gaye AT (2013a) Interannual variability of rainfall over the Sahel based on multiple regional climate models simulations. Theor Appl Climatol 113:351–362. doi:10.1007/s00704-012-0791-y

Diallo I, Sylla MB, Gaye AT, Camara M (2013b) Intercomparaison de la climatologie et de la variabilité interannuelle de la pluie simulée au Sahel par les modèles climatiques régionaux. Sécheresse 24:96–106. doi:10.1684/sec.2013.0382

Drobinski P et al (2009) On the late northward propagation of the West African monsoon in summer 2006 in the region of Niger/Mali. J Geophys Res 114:D09108

Flaounas E, Janicot S, Bastin S, Roca R (2012) The West African monsoon onset in 2006: sensitivity to surface albedo, orography, SST and synoptic scale dry-air intrusion using WRF. Clim Dyn 38:685–708. doi:10.1007/s00382-011-1255-2

Garcia-Carreras L, Marsham JH, Bain DJ, Milton S, Saci A, Salah-Ferroudj M, Ouchene B, Washington R (2013) The impact of convective cold pool outflows on model biases in the Sahara. Geophys Res Lett 40:1647–1652. doi:10.1002/grl50239

Gbobaniyi E, Sarr A, Sylla MB, Diallo I, Lennard C, Diedhiou A et al (2013) Climatology, annual cycle and interannual variability of precipitation and temperature in CORDEX regional climate models simulation over West Africa. Inter J Climatol. doi:10.1002/joc.3834

Giorgi F, Jones C, Asrar G (2009) Addressing climate information needs at the regional level: the CORDEX framework. World Meteorol Organ Bull 58:175–183. http://wcrp.ipsl.jussieu.fr/RCD_Projects/CORDEX/CORDEX_giorgi_WMO.pdf

Gu GJ, Adler RF (2004) Seasonal evolution and variability associated with the West African monsoon system. J Clim 17:3364–3377

Hagos SM, Cook KH (2007) Dynamics of the West African monsoon jump. J Clim 20:5264–5284

Harris I, Jones PD, Osborn TJ, Lister DH (2012) Updated high-resolution grids of monthly climatic observations—the CRU TS3.10 dataset. Int J. doi:10.1002/joc.3711

Hernández-Díaz L, Laprise R, Sushama L, Martynov A, Winger K, Dugas B (2013) Climate simulation over the CORDEX-Africa domain using the fifth generation Canadian Regional Climate Model (CRCM5). Clim Dyn 40:1415–1433. doi:10.1007/s00382-012-1387-z

Hourdin F, Mustat I, Guichard F, Ruti PM, Favot F, Pham MMA, Grandpeix JY, Polcher J, Marquet P, Boone A, Lafore JP, Redelsperger JL, Dell'Aquilla A, Losada Doval T, Traore AK, Galle H (2010) AMMA-model intercomparison project. Bull Am Meteorol Soc. doi:10.1175/2009BAMS2791.1

Huffman GJ, Adler RF, Bolvin DT, Gu G, Nelkin EJ, Bowman KP, Hong Y, Stocker EF, Wolff DB (2007) The TRMM multisatellite precipitation analysis (TMPA): quasi-global, multiyear, combined-sensor precipitation estimates at fine scales. J Hydrometeorol 8(1):38–55. doi:10.1175/JHM560.1

Huffman GJ, Adler RF, Bolvin DT, Gu G (2009) Improving the global precipitation record: GPCP version 2.1. Geophys Res Lett 36(17):L17,808

Janicot S, Caniaux G, Chauvin F, de Coetlogon G, Fontaine B, Hall N, Killadis G, Lafore J-P, Lavaysse C, Lavender SL, Leroux S, Marteau R, Mounier F, Philippon N, Roehrrig R, Sultan B, Taylor CM (2011) Intraseasonal variability of the West African monsoon. Atmos Sci Lett 12:58–66. doi:10.1002/asl.280

Kalnay E et al (1996) The NCEP/NCAR 40-year reanalysis project. Bull Am Meteorol Soc 83:1631–1643

Legates DR, Willmott CJ (1990) Mean seasonal and spatial variability in gauge-corrected, global precipitation. Int J Climatol 10:111–127

Mitchell TD, Jones PD (2005) An improved method of constructing a database of monthly climate observations and associated high resolution grids. Int J Climatol 25:693–712. doi:10.1002/joc.1181

Moufouma-Okia W, Rowell DP (2010) Impact of soil moisture initialisation and lateral boundary conditions on regional climate model simulations of the West African Monsoon. Clim Dyn 35:213–229. doi:10.1007/s00382-009-0638-0

Nicholson SE (2008) The intensity, location and structure of the tropical rainbelt over West Africa as factors in inter annual variability. Int J Climatol 28:1775–1785

Nicholson SE (2009a) On the factors modulating the intensity of the tropical rainbelt over West Africa. Int J Climatol 29:673–689

Nicholson SE (2009b) A revised picture of the structure of the "monsoon" and land ITCZ over West Africa. Clim Dyn 32:1155–1171

Nicholson SE (2013) The West African Sahel: a review of recent studies on the rainfall regime and its interannual variability. Meteorology. Volume 2013, Article ID 453521, 32 pages. doi:10.1155/2013/453521

Nikulin G, Jones C, Samuelsson P, Giorgi F, Asrar G, Büchner M, Cerezo-Mota R, Christensen OB, Déqué M, Fernandez J, Hänsler A, van Meijgaard E, Sylla MB, Sushama L (2012) Precipitation climatology in an ensemble of CORDEX-Africa regional climate simulations. J Clim 6057–6078. doi:10.1175/JCLI-D-11-00375.1

Okumura Y, Xie SP (2004) Interaction of the Atlantic equatorial cold tongue and the African monsoon. J Clim 17:3589–3602

Ramel R, Gallee H, Messager C (2006) On the northward shift of the West African monsoon. Clim Dyn. doi:10.1007/s00382-005-0093-5

Reynolds RW, Rayner NA, Smith TM, Stockes DC, Wang W (2003) An improved in situ and satellite SST analysis for climate. J Clim 15:1609–1625

Rienecker MM, Suarez MJ, Gelaro R (2011) MERRA—NASA's modern-era retrospective analysis for research and applications. J Clim 24:3624–3648. doi:10.1175/JCLI-D-11-00015.1

Sijikumar S, Roucou P, Fontaine B (2006) Monsoon onset over Sudan-Sahel: simulation by the regional scale model MM5. Geophys Res Lett 33:L03814. doi:10.1029/2005GL024819

Sultan B, Janicot S (2003) The West African monsoon dynamics. Part II: the "preonset" and "onset" of the summer monsoon. J Clim 16:3407–3427

Sylla MB, Gaye AT, Pal JS, Jenkins GS, Bi XQ (2009) High resolution simulations of West African climate using Regional Climate Model (RegCM3) with different lateral boundary conditions. Theor Appl Climatol 98:293–314. doi:10.1007/s00704-009-0110-4

Sylla MB, Dell'Aquila A, Ruti PM, Giorgi F (2010a) Simulation of the intraseasonal and the interannual variability of rainfall over West Africa with RegCM3 during the monsoon period. Int J Climatol 30:1865–1883. doi:10.1002/joc.2029

Sylla MB, Coppola E, Mariotti L, Giorgi F, Ruti PM, Dell'Aquila A, Bi X (2010b) Multiyear simulation of the African climate using a regional climate model (RegCM3) with the high resolution ERA-interim reanalysis. Clim Dyn 35:231–247. doi:10.1007/s00382-009-0613-9

Sylla MB, Giorgi F, Ruti PM, Calmanti S, Dell'Aquila A (2011) The impact of deep convection on the West African summer monsoon climate: a regional climate model sensitivity study. Q J R Meteorol Soc 137:1417–1430. doi:10.1002/qj.853

Sylla MB, Giorgi F, Coppola E, Mariotti L (2013a) Uncertainties in daily rainfall over Africa: assessment of gridded observation products and evaluation of a regional climate model simulation. Int J Climatol 33:1805–1817. doi:10.1002/joc.3551

Sylla MB, Diallo I, Pal JS (2013b) West African monsoon in state-of-the-science regional climate models. Intech Book Chapter: Climate variability—regional and thematic patterns, ISBN 980-953-307-816-3

Thorncroft CD, Blackburn M (1999) Maintenance of the African easterly jet. Q J R Meteorol Soc 125:763–786

Thorncroft CD, Hanh N, Zhang CD, Peyrille P (2011) Annual cycle of the West African monsoon: regional circulations and associated water vapor transport. Q J R Meteorol Soc 137:129–147. doi:10.1002/qj.728

Uppala S, Dee D, Kobayashi S, Berrisford P, Simmons A (2008) Towards a climate data assimilation system: status update of ERA-interim. ECMWF Newslett 115:12–18

Vellinga M, Arribas A, Graham R (2013) Seasonal forecast for regional onset of the West African monsoon. Clim Dyn 40:3047–3070. doi:10.1007/s00382-012-1520-z

Walters DN et al (2011) The Met Office Unified Model global atmosphere 3.0/3.1 and JULES global land 3.0/3.1 configurations. Geosci Model Dev 4:919–941. doi:10.5194/gmd-4-919-2011

Yamada TJ, Kanae S, Oki T, Hirabayashi Y (2012) The onset of the West African monsoon simulated in a high-resolution atmospheric general circulation model with reanalyzed soil moisture fields. Atmos Sci Lett 13:103–107. doi:10.1002/asl.367